

---

---

# Robust Quantification of Phosphodiesterase-4D in Monkey Brain with PET and $^{11}\text{C}$ -Labeled Radioligands That Avoid Radiometabolite Contamination

Meijuan Jiang\*, Shiyu Tang\*, Madeline D. Jenkins, Adrian C. Lee, Bruny Kenou, Carson Knoer, Jose Montero Santamaria, Shawn Wu, Jehi-San Liow, Sami S. Zoghbi, Paolo Zanotti-Fregonara, Robert B. Innis, Sanjay Telu, and Victor W. Pike

*Molecular Imaging Branch, National Institute of Mental Health, National Institutes of Health, Bethesda, Maryland*

---

Phosphodiesterase-4D (PDE4D) has emerged as a significant target for treating neuropsychiatric disorders, but no PET radioligand currently exists for robustly quantifying human brain PDE4D to assist biomedical research and drug discovery. A prior candidate PDE4D PET radioligand, namely [ $^{11}\text{C}$ ]T1650, failed in humans because of poor time stability of brain PDE4D-specific signal (indexed by total volume of distribution), likely due to radiometabolites accumulating in brain. Its nitro group was considered to be a source of the brain radiometabolites. **Methods:** We selected 5 high-affinity and selective PDE4D inhibitors, absent of a nitro group, from our prior structure-activity relationship study for evaluation as PET radioligands. **Results:** All 5 radioligands were labeled with  $^{11}\text{C}$  (half-time, 20.4 min) in useful yields and with high molar activity. All displayed sizable PDE4D-specific signals in rhesus monkey brain. Notably, [ $^{11}\text{C}$ ]JMJ-81 and [ $^{11}\text{C}$ ]JMJ-129 exhibited excellent time stability of signal (total volume of distribution). Furthermore, as an example, [ $^{11}\text{C}$ ]JMJ-81 was found to be free of radiometabolites in ex vivo monkey brain, affirming that this radioligand can provide robust quantification of brain PDE4D with PET. **Conclusion:** Given their high similarity in structures and metabolic profiles, both [ $^{11}\text{C}$ ]JMJ-81 and [ $^{11}\text{C}$ ]JMJ-129 warrant further evaluation in human subjects. [ $^{11}\text{C}$ ]JMJ-129 shows a higher PDE4D specific-to-nonspecific binding ratio and will be the first to be evaluated.

**Key Words:**  $^{11}\text{C}$ ; PET; phosphodiesterase-4D (PDE4D); inhibitors

**J Nucl Med** 2024; 65:788–793

DOI: 10.2967/jnumed.123.266750

---

**P**ET is a powerful molecular imaging technique that is used for biomedical research, drug development, and diagnosis (1,2). PET can use appropriately designed radioligands to provide quantitative measures of biochemical targets and information on the kinetics of physiologic and biochemical processes. Targets for PET imaging in brain frequently include neurotransmitter receptors, transporters, plaques, and enzymes. A PET camera is unable to distinguish the sources of radioactivity between parent (unchanged) radioligand and its radiometabolites. Thus, a highly important prerequisite for

quantifying brain imaging targets is that PET radioligands should be free of radiometabolite contamination.

Consisting of 11 families, cyclic nucleotide phosphodiesterases are enzymes that degrade major secondary messengers, such as adenosine monophosphate and cyclic guanosine monophosphate. Therefore, phosphodiesterases play critical roles in various physiologic processes such as cell growth, metabolism, inflammation, and apoptosis (3,4). Phosphodiesterase-4 (PDE4) specifically hydrolyzes cyclic adenosine monophosphate and has 4 subtypes (A, B, C, and D) that are highly conserved in their catalytic domains (4). PDE4 inhibitors have become of interest for the potential treatment of neuropsychiatric disorders, such as clinical depression and cognitive impairment (5–9). However, nausea and emesis quickly emerged as intolerable side effects in the early development of rolipram, a subtype-nonspecific PDE4 inhibitor, as a potential antidepressant drug. These side effects have been ascribed to low selectivity for binding among the different PDE4 subtypes and have provided impetus for developing subtype-selective PDE4 inhibitors (10–12). In particular, inhibitors selective for phosphodiesterase-4D (PDE4D; i.e., PDE4D7–S129D, a dimeric isoform of PDE4D that contains a UCR1 mutation [S129D] that mimics protein kinase A phosphorylation [in our earlier publications, half-maximal effective concentrations were described as  $IC_{50}$  values]) are being developed as cognition enhancers and as drugs for the treatment of fragile X syndrome (clinical trial phase III) (13–16). A PET radioligand for imaging and quantifying PDE4D in human brain could therefore become a valuable tool for biomedical research and drug development.

Recently, significant advances have been made on developing radioligands for imaging phosphodiesterases across families 1, 2, 4, 5, 7, and 10 (4,17,18). Typically, PDE4 is imaged in human subjects with PET using the subtype-nonspecific radioligand [ $^{11}\text{C}$ ](R)-rolipram (19–21). A PDE4B-prefering PET radioligand, code-named [ $^{18}\text{F}$ ]PF-06445974, has recently been developed and evaluated in human subjects (22,23). However, there is so far no PDE4D-selective radioligand for robust quantitative PET imaging of this subtype in human brain. Earlier, we explored several chemotypes as PDE4D inhibitors and potential PET radioligands. Four compounds with alkoxy-pyridinyl cores were selected and then successfully labeled with cyclotron-produced  $^{11}\text{C}$  (half-time, 20.4 min) for PET imaging of PDE4D in monkey brain (24). Among these four, the most promising candidate radioligand, [ $^{11}\text{C}$ ]T1650 (Fig. 1), failed in subsequent human PET experiments. Total volume of distribution ( $V_T$ ) measurements showed time instability that impeded the robust measurements of PDE4D

---

Received Sep. 27, 2023; revision accepted Jan. 5, 2024.  
For correspondence or reprints, contact Victor W. Pike (pikev@mail.nih.gov) or Sanjay Telu (sanjay.tel@nih.gov).  
\*Contributed equally to this work.  
Published online Feb. 29, 2024.  
COPYRIGHT © 2024 by the Society of Nuclear Medicine and Molecular Imaging.

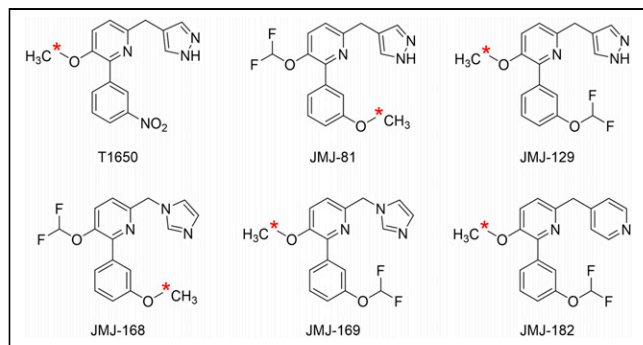


**FIGURE 1.** Chemical structures of T1650 and 5 new PDE4D radioligand candidates. Asterisks denote sites for  $^{11}\text{C}$  labeling.

density. An accumulation of radiometabolites in brain, originating from either brain or periphery, was likely responsible for this instability (24). Thus, further structural changes to T1650 were deemed to be needed to obtain a successful PDE4D radioligand.

Thereafter, we embarked on a medicinal chemistry campaign to study structure–activity relationships for PDE4D inhibitory potency around T1650 as the lead compound. The efficiency of this campaign was enhanced by the discovery of an empiric equation that was able to describe and predict PDE4D half-maximal effective concentrations from 2-dimensional structures composed of 4 substructure fragments (25). We hypothesized that the reduction of the nitro group in [ $^{11}\text{C}$ ]T1650 might be a source of radiometabolites in human brain. From this preceding structure–activity relationship study, we herein selected 5 high-affinity PDE4D selective inhibitors with no nitro group (Fig. 1) to be labeled in the methoxy position with  $^{11}\text{C}$  and to be compared as PET radioligands in monkeys. These inhibitors are encoded JMJ-81, JMJ-129, JMJ-168, JMJ-169, and JMJ-182, which correspond to inhibitors 9, 5, 43, 30, and 49, respectively, in our prior publication (25).

## MATERIALS AND METHODS

The experimental details can be found in the supplemental data (supplemental materials are available at <http://jnm.snmjournals.org>) (24–36).

## RESULTS

### PET Radioligand Candidacy

Table 1 summarizes key physicochemical and pharmacologic properties (adapted from our previous work (25)) for the 5 selected PDE4D inhibitors with respect to PET radioligand candidacy (37). All 5 inhibitors have high scores of multiparameter optimization for central nervous system PET radioligands (26) for predicted high efficacy, higher affinity for PDE4D (half-maximal effective concentration, 1.1–2.7 nM) than T1650 (half-maximal effective concentration, 3.5 nM) for potentially high specific binding, very high selective binding to PDE4D over PDE4B, and moderate calculated lipophilicities expected to be conducive to good blood–brain barrier permeability. All 5 inhibitors carry an aryl methoxy group, which we considered to be amenable to labeling with  $^{11}\text{C}$  (half-time, 20.4 min) and which is often (but not always) a favored labeling site for avoiding troublesome radiometabolites (38).

Off-target binding activities against a panel of G-protein-coupled receptors and other binding sites (a total of 46 receptor and sites) were tested in vitro by the National Institute of Mental

Health Psychoactive Drug Screening Program (39) for JMJ-81, JMJ-129, JMJ-168, and JMJ-169. The results did not reveal any high binding affinities (Supplemental Tables 1 and 2). The most potent hit in the panel was translocator protein 18 kDa for both JMJ-81 and JMJ-129. The inhibition constants are 1,819 nM and 1,392 nM, respectively, which are insignificant compared with the strong binding affinities for PDE4D.

### Radiochemical Syntheses, Purifications, and Formulations of Radioligands

Hydroxy precursors (1–5) were synthesized for the preparation of the radioligands (Supplemental Scheme 1). These precursors were fully characterized and over 95% pure on analytic high-performance liquid chromatography (HPLC) (Supplemental Figs. 1–25). As shown in Figure 2, the synthesized respective hydroxy precursor (selected as appropriate from 1 to 5) was treated with no-carrier-added [ $^{11}\text{C}$ ]iodomethane (28), followed by rapid separation with reversed-phase HPLC. Separation conditions are summarized in Supplemental Tables 3 and 4. Each isolated radioligand was formulated in ethanol-saline (1:10 v/v) for intravenous injection into monkeys for PET imaging. All radioligands were obtained in good radiochemical yields with high molar activities ( $>269$  GBq/ $\mu\text{mol}$ , Supplemental Table 5) and high radiochemical purities ( $>99.4\%$ , Supplemental Table 6). Radioligand identities were confirmed by coinjection with matching reference inhibitor onto analytic radio-HPLC and by liquid chromatography–mass spectrometry/mass spectrometry–mass spectrometry of residual carrier after radioactive decay. Supplemental Figures 26–35 show the representative HPLC radiochromatograms and mass spectrometry spectra. All formulated radioligand solutions were chemically and radiochemically stable for at least 1 h at room temperature on radio-HPLC analysis. The lipophilicities of the radioligands were also measured (Table 1) and considered conducive for good blood–brain barrier permeability (26,38).

### Comparison of Candidate Radioligands for PET Imaging of Monkey Brain

As shown in Figure 3A, after intravenous injection of [ $^{11}\text{C}$ ]JMJ-81 at baseline, whole-brain radioactivity rapidly peaked at 3.2 SUV after 7 min and then decreased slowly to 1.3 SUV at 120 min. In another experiment, rolipram (0.5 mg/kg) was administered as a blocking agent to the same monkey at 5 min before [ $^{11}\text{C}$ ]JMJ-81. The time–activity curve for whole brain peaked earlier and higher and then dropped more quickly than at baseline. This difference indicated the presence of high PDE4-specific binding in the baseline experiment. The radiometabolite-corrected arterial input functions for [ $^{11}\text{C}$ ]JMJ-81 in both experiments (Fig. 3B) show that unchanged [ $^{11}\text{C}$ ]JMJ-81 cleared rapidly from arterial plasma, with little difference between experiments. Compartmental modeling corrects for the difference in blood flow and exposure of the brain to unchanged radioligand under baseline and blocked conditions by calculating  $V_T$ , a measure of total binding (specific and nondisplaceable) (36).  $V_T$  values from 2-tissue-compartment modeling for whole brain and selected brain regions at 90 min after injection of [ $^{11}\text{C}$ ]JMJ-81 (Fig. 3C) showed clear decreases from baseline  $V_T$  values after blocking of PDE4D with rolipram, thereby confirming the presence of a high proportion of specific binding at baseline. The same experimental conditions were repeated in a second monkey with similar results (Supplemental Fig. 36), except that the rolipram dose was reduced from 0.5 to 0.2 mg/kg to avoid any potential for emetic side effect. The other 4 radioligands also

TABLE 1

Physicochemical Properties, Pharmacologic Properties, and PET Imaging Parameters in Monkeys of 5 Selected PDE4D Radioligands and Previously Reported (24) PDE4D Ligand [ $^{11}\text{C}$ ]T1650

Radioligand	CNS PET MPO	$EC_{50}$ (nM)		Selectivity (B/D)	$c\text{Log}D_{7.4}$	$m\text{Log}D_{7.4}$	$f_p$ (%)	$V_{ND}$	$BP_{ND}$
		PDE4D	PDE4B						
[ $^{11}\text{C}$ ]T1650	3.9	3.5	1120	320	3.48	2.89	$6.7 \pm 0.7$	3.58	1.2
[ $^{11}\text{C}$ ]JMJ-81	4.2	$2.7 \pm 0.5$	$521 \pm 46$	193	2.90	3.15	$5.7 \pm 0.8$	3.3, 3.4	1.2, 0.61
[ $^{11}\text{C}$ ]JMJ-129	4.3	$1.4 \pm 0.01$	$1070 \pm 14$	793	2.90	3.28	$5.8 \pm 0.7$	3.5, 4.3	2.4, 1.0
[ $^{11}\text{C}$ ]JMJ-168	4.1	2.1	513	242	3.17	2.73	$6.8 \pm 0.5$	4.0, 5.3	0.69, 0.27
[ $^{11}\text{C}$ ]JMJ-169	4.1	1.1	593	559	3.17	2.82	$8.4 \pm 0.8$	5.2, 3.9	0.57, 2.2
[ $^{11}\text{C}$ ]JMJ-182	3.4	2.0	1340	670	3.28	3.33	$2.9 \pm 0.2$	4.3, 3.7	0.59, 0.44

CNS PET MPO = multiparameter optimization value for central nervous system PET radioligand (estimated as in (26));  $EC_{50}$  = half-maximal effective concentration; B/D = ratio of  $EC_{50}$  for PDE4B over that for PDE4D;  $c\text{Log}D_{7.4}$  = computed lipophilicity for *n*-octanol/buffer solution distribution coefficient at pH 7.4;  $m\text{Log}D_{7.4}$  = experimentally measured lipophilicity;  $f_p$  = plasma free fraction; PDE4B = PDE4B1-S133D, dimeric isoform of PDE4B that contains UCR1 mutation (S133D) that mimics protein kinase A phosphorylation.

Data for multiparameter optimization for central nervous system PET radioligand scoring (i.e., PDE4D  $EC_{50}$ , PDE4B  $EC_{50}$ , B/D, and  $c\text{log}D_{7.4}$ ) are sourced from our previous reports (24,25). Binding assays were repeated ( $n = 2$ ) for JMJ-81 and JMJ-129.  $c\text{Log}D_{7.4}$  values were calculated with Pallas software;  $m\text{log}D_{7.4}$  values were measured with radioligands ( $n = 6$ ). Plasma free fraction was measured and averaged with monkey plasma ( $n = 4$  or greater).  $V_{ND}$  and  $BP_{ND}$  were measured in 2 monkeys except in one monkey for [ $^{11}\text{C}$ ]T1650, in which rolipram was used as blocking agent at 0.5 mg/kg for first monkey studied with [ $^{11}\text{C}$ ]JMJ-81 and at 0.2 mg/kg for all other experiments.

showed specific binding to PDE4 in the brain with a rolipram dose of 0.2 mg/kg (Supplemental Figs. 37–40).

Furthermore, the whole-brain nondisplaceable binding volume of distribution ( $V_{ND}$ ) and specific-to-nondisplaceable ratio ( $BP_{ND}$ ) were assessed with a Lassen plot (33,40) using the regional  $V_T$  values from the above baseline and blocked studies. In the 2 [ $^{11}\text{C}$ ]JMJ-81 monkeys, acceptable receptor occupancies with rolipram were reached (92% with 0.5 mg/kg and 65% with 0.2 mg/kg) and correlation coefficients ( $R^2$ ) were high (0.996 and 0.874, respectively) so as to give reliable results (Fig. 4A). Receptor occupancies of [ $^{11}\text{C}$ ]JMJ-129 were 93% ( $R^2 = 0.996$ ) and 74% ( $R^2 = 0.941$ ) (Fig. 4B). Similarly, brain  $V_{ND}$  and  $BP_{ND}$  values were also assessed for the other 3 radioligands (Supplemental Fig. 41). To allow comparison of the 5 radioligands, the measured plasma free fraction,  $V_{ND}$ , and  $BP_{ND}$  are summarized in Table 1. Plasma free fraction was highest for [ $^{11}\text{C}$ ]JMJ-169 (8.4%) and lowest for [ $^{11}\text{C}$ ]JMJ-182 (2.9%), which can be largely explained by their

relative lipophilicities (41).  $V_{ND}$  was similar across the 5 radioligands, ranging from 3.3 to 5.3. The highest average  $BP_{ND}$  values were observed for [ $^{11}\text{C}$ ]JMJ-129 (1.7) and [ $^{11}\text{C}$ ]JMJ-169 (1.4). A moderate average  $BP_{ND}$  (0.9) was observed for [ $^{11}\text{C}$ ]JMJ-81, whereas the lowest average  $BP_{ND}$  (0.5) was observed for [ $^{11}\text{C}$ ]JMJ-168 and [ $^{11}\text{C}$ ]JMJ-182. These values do not correlate well with the inhibitory potencies of the radioligands measured in vitro (Table 1), likely because  $BP_{ND}$  is also influenced by nonspecific binding.

For robust PDE4D quantification,  $V_T$  values should become stable with scan duration. Such time stabilization of  $V_T$  is a strong indicator that the measured radioligand signal is free of contamination by radiometabolites and is therefore reliable. The  $V_T$  values for whole brain, frontal cortex, and cerebellum for [ $^{11}\text{C}$ ]JMJ-81 in 2 monkeys (Figs. 4C) plateaued within 90%–110% of the terminal value after 90 min of scanning. The curves for [ $^{11}\text{C}$ ]JMJ-129 also stabilized after 90 min (Figs. 4D). By contrast, curves for the other 3 radioligands did not plateau after 90 min in either monkey, indicating possible accumulation of radiometabolites in brain (Supplemental Fig. 42). Therefore, [ $^{11}\text{C}$ ]JMJ-81 and [ $^{11}\text{C}$ ]JMJ-129 were considered worthy of further study.

#### In Vivo Selectivity of Binding to PDE4D in Monkey Brain

Use of the pan-PDE4 inhibitor, rolipram, as a blocking agent provides evidence for binding of the radioligands to all PDE4s, not specifically to the 4D subtype. To test the selectivity of the binding of [ $^{11}\text{C}$ ]JMJ-81 and [ $^{11}\text{C}$ ]JMJ-129 to PDE4D in vivo, a PDE4D-selective inhibitor (BPN14770) (15) was also used. Much faster brain washout (Supplemental Fig. 43) and reduced whole-brain and regional  $V_T$  values (Fig. 5A) were observed for [ $^{11}\text{C}$ ]JMJ-81 and [ $^{11}\text{C}$ ]JMJ-129 after blockade of PDE4D with BPN14770 than at baseline. The  $BP_{ND}$  values assessed from Lassen plots were 1.1 for [ $^{11}\text{C}$ ]JMJ-81 and 2.0 for [ $^{11}\text{C}$ ]JMJ-129 (Supplemental Fig. 43) and similar to those averaged from rolipram blocking experiments (0.9 and 1.7, respectively, Table 1). The  $BP_{ND}$  value, as well as PET images (Figs. 5B), well

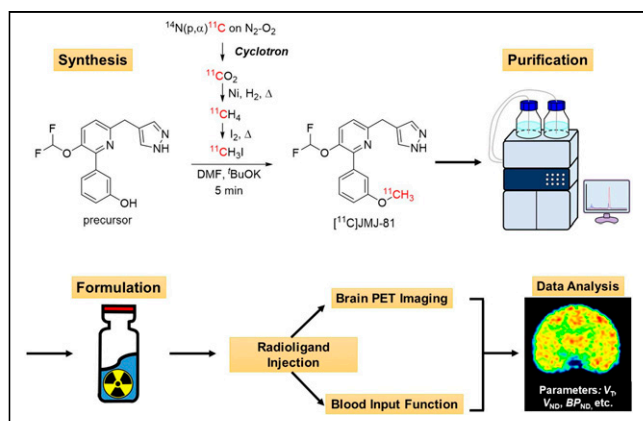
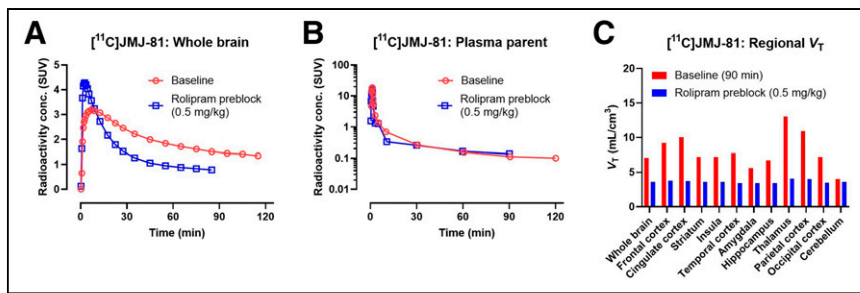


FIGURE 2. Illustration of radioligand production and evaluation. DMF = dimethylformamide.



**FIGURE 3.** (A and B) Time-activity curves after injection of [<sup>11</sup>C]JMJ-81 for monkey brain (A) and unchanged radioligand in plasma (B) at baseline and after block by rolipram (0.5 mg/kg, intravenously) in same monkey. (C)  $V_T$  values at 90 min after injection of [<sup>11</sup>C]JMJ-81 across monkey brain regions at baseline and after block by rolipram (0.5 mg/kg intravenously). SUV is calculated as radioactivity in brain (Bq) per g of brain divided by injected activity (Bq) per g of body weight (36).

demonstrated the selective binding of [<sup>11</sup>C]JMJ-81 and [<sup>11</sup>C]JMJ-129 to PDE4D in whole brain and frontal cortex, which is an important region for cognition.

### Study of Radiometabolites in Rats

To evaluate the possibility of radiometabolite accumulation in brain, the stabilities of [<sup>11</sup>C]JMJ-81 and [<sup>11</sup>C]JMJ-129 were assessed in rats in vitro and ex vivo and compared with those of [<sup>11</sup>C]T1650 (24). All 3 radioligands were stable after incubation in vitro with whole blood and plasma for at least 30 min (Fig. 6A; Supplemental Fig. 44). However, when incubated with fresh brain homogenates, [<sup>11</sup>C]T1650 remained only 59% unchanged (Supplemental Fig. 45) (24) whereas [<sup>11</sup>C]JMJ-81 and [<sup>11</sup>C]JMJ-129 remained completely unchanged. Given their structures (Fig. 1), we consider that the absence of the nitro group likely increased the metabolic stabilities of the new radioligands, [<sup>11</sup>C]JMJ-81 and [<sup>11</sup>C]JMJ-129, over that of [<sup>11</sup>C]T1650. All 3 radioligands showed appreciable proportions of radioactivity as radiometabolites in plasma and brain ex vivo at 30 min after intravenous injection (Fig. 6B; Supplemental Figs. 46 and 47) (24).

### Study of Radiometabolites in Monkey

Because we found radiometabolites of [<sup>11</sup>C]JMJ-81 and [<sup>11</sup>C]JMJ-129 in rat brain, we more deeply investigated the

possibility of radiometabolites in monkey brain. Exemplified with [<sup>11</sup>C]JMJ-81, 2 plasma samples and 4 random regional brain samples were collected at 30 min after radioligand injection and analyzed with radio-HPLC. The results showed that although unchanged [<sup>11</sup>C]JMJ-81 was only 22% of the total radioactivity in plasma, all radioactivity in brain (99% ± 0.7%) was unchanged [<sup>11</sup>C]JMJ-81 (Fig. 6C). Thus, unlike rat brain, monkey brain was found not to accumulate radiometabolites to any significant extent. These findings affirm that [<sup>11</sup>C]JMJ-81 provides robust measures of PDE4D in monkey brain that are free of contamination from radiometabolites.

Given the high similarity in their structures and radiometabolic profiles, [<sup>11</sup>C]JMJ-129 should behave similarly. Similarity has been confirmed since submission of this paper.

### DISCUSSION

The selectivity of our ligands to PDE4D over other PDE4 subtypes lies in a single phenylalanine residue in UCR2 of PDE4D (24,25). This UCR2 residue is unique to primates and is recognized for binding by our inhibitors. By contrast, the same position in PDE4A–C is occupied by a tyrosine residue and thus confers low affinity on our PDE4D inhibitors. In previous reports (13,15), PDE4B was demonstrated to be a good representative of PDE4A–C to test the pan-subtype selectivity for inhibitors with the same mechanism. Also, because UCR2 is unique to PDE4, PDE4D-selective inhibitors were also selective over other PDE families (13). These results should apply to our ligands because they have similar structural skeletons and have high selectivity to PDE4D over PDE4B. In addition, binding to 46 brain receptors and binding sites other than PDE families was tested for our ligands, and no significant off-target binding was found. Altogether, our ligands showed excellent selectivity for PDE4D in vitro.

Exploration of the PDE4D pharmacology of our inhibitors in

mice would be futile because the critical residue in mouse PDE4D is also tyrosine, as in PDE4A–C (13,15). Monkey was therefore selected as the species for evaluation of our candidate PET radioligands. In addition, the size of monkey brain usefully allows comparison of PET signals from different brain regions and also allows derivation of  $V_{ND}$ . Of the 5 candidates, both [<sup>11</sup>C]JMJ-129 and [<sup>11</sup>C]JMJ-81 demonstrated high and moderate  $BP_{ND}$ , good time stability, and good in vivo selectivity to PDE4D in monkey brain. A high  $BP_{ND}$  was also observed for [<sup>11</sup>C]JMJ-169, but  $V_T$  time stability was less favorable than for [<sup>11</sup>C]JMJ-129 and [<sup>11</sup>C]JMJ-81.

Ex vivo analysis of brain tissues detected radiometabolites of both [<sup>11</sup>C]JMJ-129 and [<sup>11</sup>C]JMJ-81 in rat brain. Given the high stability of [<sup>11</sup>C]JMJ-81 and [<sup>11</sup>C]JMJ-129 in rat brain in vitro, we conclude that the radiometabolites of [<sup>11</sup>C]JMJ-81 and [<sup>11</sup>C]JMJ-129 had only a peripheral origin. This likely differs

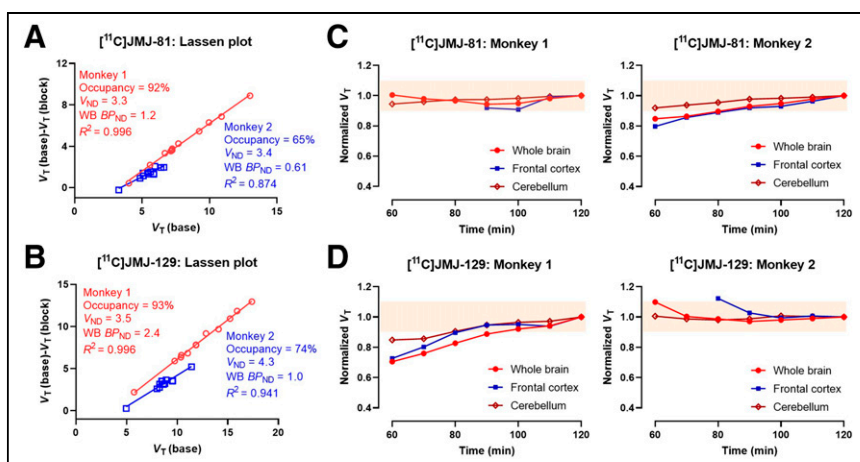


**FIGURE 4.** (A and B) Lassen plots for whole brain in 2 monkeys for [<sup>11</sup>C]JMJ-81 (A) and [<sup>11</sup>C]JMJ-129 (B), based on  $V_T$  measures from 2-tissue-compartment modeling. (C and D)  $V_T$  time-stability curves for whole brain, frontal cortex, and cerebellum for [<sup>11</sup>C]JMJ-81 (C) and [<sup>11</sup>C]JMJ-129 (D) from 2 monkeys.  $V_T$  values are normalized to end of scan values. Rolipram dose was 0.5 mg/kg for monkey 1 in [<sup>11</sup>C]JMJ-81 experiment only. Other experiments used rolipram at 0.2 mg/kg. WB = whole brain.

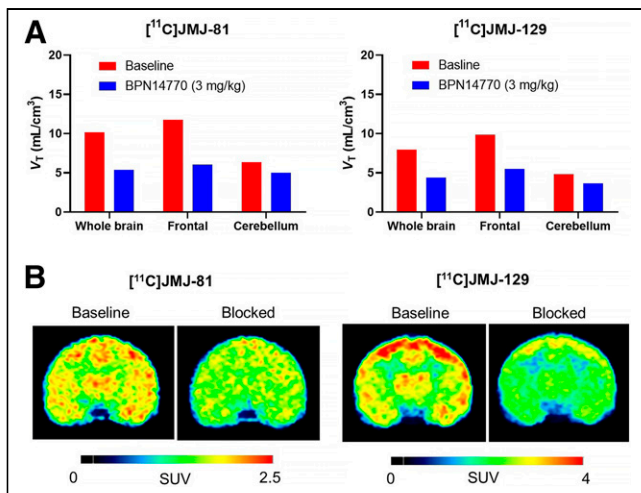


**FIGURE 5.** (A)  $V_T$  estimated by Logan analysis of regional monkey brain data for [ $^{11}\text{C}$ ]JMJ-81 and [ $^{11}\text{C}$ ]JMJ-129 at baseline and after PDE4D block with BPN14770 (3 mg/kg, intravenously). (B) PET images of radioactivity concentration (SUV) for [ $^{11}\text{C}$ ]JMJ-81 and [ $^{11}\text{C}$ ]JMJ-129 in monkey brain at baseline and after PDE4D block. Radioactivity concentrations were averaged from 20 to 60 min.

from [ $^{11}\text{C}$ ]T1650, whose radiometabolites in brain are suspected to originate from both brain and peripheral organs, as discussed previously (24). The level of radiometabolites from [ $^{11}\text{C}$ ]JMJ-81 was negligible in monkey brain. It should be recalled that rodent brain PDE4D does not bind these radioligands with any great affinity. Therefore, the radioactivity in rat brain is all nondisplaceable and therefore at a lower concentration than if there were PDE4D-specific binding. This renders the radiometabolites more noticeable—that is, as a higher proportion of total radioactivity than if there were additionally PDE4D-specific binding. Moreover, we

observed that radiochromatographic profiles were very different between rat and monkey plasma. For example, at 30 min after injection, [ $^{11}\text{C}$ ]JMJ-81 and [ $^{11}\text{C}$ ]JMJ-129 have higher proportions of radioactivity as unchanged radioligand in monkey plasma than in rat plasma (Supplemental Figs. 47 and 48), suggesting that [ $^{11}\text{C}$ ]JMJ-81 and [ $^{11}\text{C}$ ]JMJ-129 metabolize more quickly in rats than in primates. For [ $^{11}\text{C}$ ]T1650, a moderately lipophilic radiometabolite fraction was found to elute on reversed-phase HPLC between the early eluting polar radiometabolites and unchanged radioligand in rat, monkey, and human plasma (Supplemental Fig. 48) (24). This fraction was comparatively negligible in monkey plasma over time for both [ $^{11}\text{C}$ ]JMJ-81 and [ $^{11}\text{C}$ ]JMJ-129 (Supplemental Fig. 49). Thus, there is a marked species difference in metabolism for these 2 radioligands. This explains why lipophilic radiometabolite accumulation for [ $^{11}\text{C}$ ]JMJ-81 in monkey brain was negligible, in accord with the observed time stability of monkey brain  $V_T$  values. Given the high [ $^{11}\text{C}$ ]JMJ-81 and [ $^{11}\text{C}$ ]JMJ-129 structural similarity, radiometabolite accumulation in monkey brain should also be negligible for [ $^{11}\text{C}$ ]JMJ-129. In all, [ $^{11}\text{C}$ ]JMJ-81 and [ $^{11}\text{C}$ ]JMJ-129 are both worthy of further evaluation in human subjects. [ $^{11}\text{C}$ ]JMJ-129 is proposed for first evaluation because it gives the higher signal-to-background ratio (higher  $BP_{ND}$ ).

## CONCLUSION

Five radioligands, designed not to have the nitro group seen in [ $^{11}\text{C}$ ]T1650, namely [ $^{11}\text{C}$ ]JMJ-81, [ $^{11}\text{C}$ ]JMJ-129, [ $^{11}\text{C}$ ]JMJ-168, [ $^{11}\text{C}$ ]JMJ-169, and [ $^{11}\text{C}$ ]JMJ-182, were successfully prepared in good yields and with high molar activities for evaluation in monkey as radioligands for imaging brain PDE4D with PET. All 5 showed sizable PDE4D-specific signals in whole brain and enzyme-rich regions. [ $^{11}\text{C}$ ]JMJ-81 and [ $^{11}\text{C}$ ]JMJ-129 showed superior signal ( $V_T$ ) time stability over the other radioligands. In vitro screening and in vivo preblocking with BPN14770 demonstrated the selectivity of the radioligands for binding to the PDE4D subtype. [ $^{11}\text{C}$ ]JMJ-81 and [ $^{11}\text{C}$ ]JMJ-129 were highly stable in fresh rat brain homogenates, unlike [ $^{11}\text{C}$ ]T1650. Moreover [ $^{11}\text{C}$ ]JMJ-81 was shown not to accumulate radiometabolites in monkey brain, thereby firmly ensuring the capability of [ $^{11}\text{C}$ ]JMJ-81 and structurally and metabolically similar [ $^{11}\text{C}$ ]JMJ-129 for robustly measuring PDE4D in monkey brain with PET. Both [ $^{11}\text{C}$ ]JMJ-81 and [ $^{11}\text{C}$ ]JMJ-129 warrant further evaluation in human subjects. [ $^{11}\text{C}$ ]JMJ-129 is proposed first for this evaluation because of its higher signal-to-noise ratio ( $BP_{ND}$ ).

## DISCLOSURE

This work was financially supported by the Intramural Research Program of NIH (NIMH) (ZIA-MH002793). No other potential conflict of interest relevant to this article was reported.

## ACKNOWLEDGMENTS

We thank Dr. John Lloyd of the NIDDK Advanced Mass Spectrometry Facility for high-resolution mass spectrometry measurements, the NIH Clinical PET Center (director, Dr. Peter Herscovitch) for radioisotope production, the NIMH Psychoactive Drug Screening Program (director, Prof. Bryan L. Roth) for off-target binding screening, and Dr. Alex Cummins (NIMH) and Dr. Mark Eldridge (NIMH) for collection of monkey brain samples.

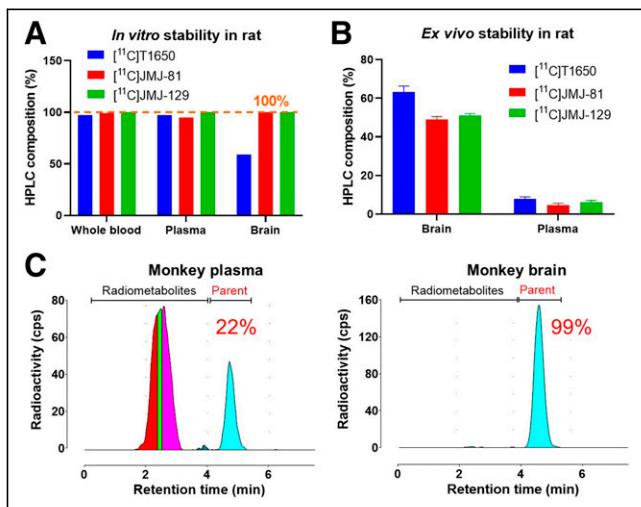


**FIGURE 6.** (A) Relative in vitro stabilities of radioligands ([ $^{11}\text{C}$ ]T1650, [ $^{11}\text{C}$ ]JMJ-81, and [ $^{11}\text{C}$ ]JMJ-129) after incubation with fresh rat whole blood, plasma, and homogenized fresh brain tissues for at least 30 min at 37°C ( $n = 1$ ). (B) Relative ex vivo stability of radioligands in rat brain and plasma at 30 min after injection ( $n = 3$ ). (C) Representative radiochromatograms for HPLC of plasma and brain harvested from monkey at 30 min after injection of [ $^{11}\text{C}$ ]JMJ-81.

## KEY POINTS

**QUESTION:** Can a radioligand be developed by modifying the previously unsuccessful ligand [ $^{11}\text{C}$ ]T1650 for PDE4D quantification in brain with PET?

**PERTINENT FINDINGS:** Five  $^{11}\text{C}$  radioligands were produced and evaluated in rhesus monkey brain with PET, and 2 of them, [ $^{11}\text{C}$ ]JMJ-81 and [ $^{11}\text{C}$ ]JMJ-129, can provide robust quantification of brain PDE4D with PET.

**IMPLICATIONS FOR PATIENT CARE:** Both [ $^{11}\text{C}$ ]JMJ-81 and [ $^{11}\text{C}$ ]JMJ-129 warrant further evaluation in human subjects.

## REFERENCES

- Gallamini A, Zwarthoed C, Borra A. Positron emission tomography (PET) in oncology. *Cancers (Basel)*. 2014;6:1821–1889.
- Hooker JM, Carson RE. Human positron emission tomography neuroimaging. *Annu Rev Biomed Eng*. 2019;21:551–581.
- Francis SH, Blount MA, Corbin JD. Mammalian cyclic nucleotide phosphodiesterases: molecular mechanisms and physiological functions. *Physiol Rev*. 2011;91:651–690.
- Sun J, Xiao Z, Haider A, et al. Advances in cyclic nucleotide phosphodiesterase-targeted PET imaging and drug discovery. *J Med Chem*. 2021;64:7083–7109.
- Wachtel H. Potential antidepressant activity of rolipram and other selective cyclic adenosine 3',5'-monophosphate phosphodiesterase inhibitors. *Neuropharmacology*. 1983;22:267–272.
- Barad M, Bourthouladze R, Winder DG, Golan H, Kandel E. Rolipram, a type IV-specific phosphodiesterase inhibitor, facilitates the establishment of long-lasting long-term potentiation and improves memory. *Proc Natl Acad Sci USA*. 1998;95:15020–15025.
- Gong B, Vitolo OV, Trinchese F, Liu S, Shelanski M, Arancio O. Persistent improvement in synaptic and cognitive functions in an Alzheimer mouse model after rolipram treatment. *J Clin Invest*. 2004;114:1624–1634.
- Bhat A, Ray B, Mahalakshmi AM, et al. Phosphodiesterase-4 enzyme as a therapeutic target in neurological disorders. *Pharmacol Res*. 2020;160:105078.
- Liu Z, Liu M, Cao Z, Qiu P, Song G. Phosphodiesterase-4 inhibitors: a review of current developments (2013–2021). *Expert Opin Ther Pat*. 2022;32:261–278.
- Bender AT, Beavo JA. Cyclic nucleotide phosphodiesterases: molecular regulation to clinical use. *Pharmacol Rev*. 2006;58:488–520.
- Kenk M, Thomas A, Lortie M, Dekemp R, Beanlands RS, Dasilva JN. PET measurements of cAMP-mediated phosphodiesterase-4 with (R)-[ $^{11}\text{C}$ ]rolipram. *Curr Radiopharm*. 2011;4:44–58.
- DeNinno MP. Future directions in phosphodiesterase drug discovery. *Bioorg Med Chem Lett*. 2012;22:6794–6800.
- Burgin AB, Magnusson OT, Singh J, et al. Design of phosphodiesterase 4D (PDE4D) allosteric modulators for enhancing cognition with improved safety. *Nat Biotechnol*. 2010;28:63–70.
- Zhang C, Xu Y, Chowdhary A, et al. Memory enhancing effects of BPN14770, an allosteric inhibitor of phosphodiesterase-4D, in wild-type and humanized mice. *Neuropsychopharmacology*. 2018;43:2299–2309.
- Gurney ME, Nugent RA, Mo X, et al. Design and synthesis of selective phosphodiesterase 4D (PDE4D) allosteric inhibitors for the treatment of fragile X syndrome and other brain disorders. *J Med Chem*. 2019;62:4884–4901.
- Partners TD. A study of BPN14770 in male adults (aged 18 to 45) with fragile X syndrome. ClinicalTrials.gov website. <https://ClinicalTrials.gov/show/NCT05358886>; Published 2022. Updated January 15, 2024. Accessed February 6, 2024.
- Schröder S, Wenzel B, Deuther-Conrad W, Scheunemann M, Brust P. Novel radioligands for cyclic nucleotide phosphodiesterase imaging with positron emission tomography: an update on developments since 2012. *Molecules*. 2016;21:650.
- Schröder S, Scheunemann M, Wenzel B, Brust P. Challenges on cyclic nucleotide phosphodiesterases imaging with positron emission tomography: novel radioligands and (pre-)clinical insights since 2016. *Int J Mol Sci*. 2021;22:3832.
- DaSilva JN, Lourenco CM, Meyer JH, Hussey D, Potter WZ, Houle S. Imaging cAMP-specific phosphodiesterase-4 in human brain with R-[ $^{11}\text{C}$ ]rolipram and positron emission tomography. *Eur J Nucl Med Mol Imaging*. 2002;29:1680–1683.
- Fujita M, Hines CS, Zoghbi SS, et al. Downregulation of brain phosphodiesterase type IV measured with  $^{11}\text{C}$ -(R)-rolipram positron emission tomography in major depressive disorder. *Biol Psychiatry*. 2012;72:548–554.
- Niccolini F, Wilson H, Pagano G, et al. Loss of phosphodiesterase 4 in Parkinson disease: relevance to cognitive deficits. *Neurology*. 2017;89:586–593.
- Zhang L, Chen L, Beck EM, et al. The discovery of a novel phosphodiesterase (PDE) 4B-preferring radioligand for positron emission tomography (PET) imaging. *J Med Chem*. 2017;60:8538–8551.
- Wakabayashi Y, Stenkrona P, Arakawa R, et al. First-in-human evaluation of [ $^{18}\text{F}$ ]PF-06445974, a PET radioligand that preferentially labels phosphodiesterase-4B. *J Nucl Med*. 2022;63:1919–1924.
- Wakabayashi Y, Telu S, Dick RM, et al. Discovery, radiolabeling, and evaluation of subtype-selective inhibitors for positron emission tomography imaging of brain phosphodiesterase-4D. *ACS Chem Neurosci*. 2020;11:1311–1323.
- Jiang M, Lu S, Telu S, Pike VW. An empirical quantitative structure-activity relationship equation assists the discovery of high-affinity phosphodiesterase 4D inhibitors as leads to PET radioligands. *J Med Chem*. 2023;66:1543–1561.
- Zhang L, Villalobos A, Beck EM, et al. Design and selection parameters to accelerate the discovery of novel central nervous system positron emission tomography (PET) ligands and their application in the development of a novel phosphodiesterase 2A PET ligand. *J Med Chem*. 2013;56:4568–4579.
- Council NR. *Guide for the Care and Use of Laboratory Animals*. 8th ed. National Academies Press; 2011.
- Larsen P, Ulin J, Dahlstrom K, Jensen M. Synthesis of [ $^{11}\text{C}$ ]iodomethane by iodination of [ $^{11}\text{C}$ ]methane. *Appl Radiat Isot*. 1997;48:153–157.
- Zoghbi S, Baldwin R, Seibyl J, Charney D, Innis R. A radiotracer technique for determining apparent pKa of receptor-binding ligands. *J Label Compd Radiopharm*. 1997;40:136–138.
- Briard E, Zoghbi SS, Imaizumi M, et al. Synthesis and evaluation in monkey of two sensitive  $^{11}\text{C}$ -labeled aryloxyamide ligands for imaging brain peripheral benzodiazepine receptors in vivo. *J Med Chem*. 2008;51:17–30.
- Zoghbi SS, Shetty HU, Ichise M, et al. PET imaging of the dopamine transporter with  $^{18}\text{F}$ -FECNT: a polar radiometabolite confounds brain radioligand measurements. *J Nucl Med*. 2006;47:520–527.
- Shrestha SS, Nelson EE, Liow J-S, et al. Fluoxetine administered to juvenile monkeys: effects on the serotonin transporter and behavior. *Am J Psychiatry*. 2014;171:323–331.
- Lassen NA, Bartenstein PA, Lammertsma AA, et al. Benzodiazepine receptor quantification in vivo in humans using [ $^{11}\text{C}$ ]flumazenil and PET: application of the steady-state principle. *J Cereb Blood Flow Metab*. 1995;15:152–165.
- Gandelman MS, Baldwin RM, Zoghbi SS, Zea-Ponce Y, Innis RB. Evaluation of ultrafiltration for the free-fraction determination of single photon emission computed tomography (SPECT) radiotracers: beta-CIT, IBF, and iomazenil. *J Pharm Sci*. 1994;83:1014–1019.
- Abi-Dargham A, Gandelman M, Zoghbi SS, et al. Reproducibility of SPECT measurement of benzodiazepine receptors in human brain with iodine-123-iomazenil. *J Nucl Med*. 1995;36:167–175.
- Innis RB, Cunningham VJ, Delforge J, et al. Consensus nomenclature for in vivo imaging of reversibly binding radioligands. *J Cereb Blood Flow Metab*. 2007;27:1533–1539.
- Pike VW. Considerations in the development of reversibly binding PET radioligands for brain imaging. *Curr Med Chem*. 2016;23:1818–1869.
- Pike VW. PET radiotracers: crossing the blood-brain barrier and surviving metabolism. *Trends Pharmacol Sci*. 2009;30:431–440.
- Besnard J, Ruda GF, Setola V, et al. Automated design of ligands to polypharmacological profiles. *Nature*. 2012;492:215–220.
- Cunningham VJ, Rabiner EA, Slifstein M, Laruelle M, Gunn RN. Measuring drug occupancy in the absence of a reference region: the Lassen plot re-visited. *J Cereb Blood Flow Metab*. 2010;30:46–50.
- Zoghbi SS, Anderson KB, Jenko KJ, Luckenbaugh DA, Innis RB, Pike VW. On quantitative relationships between drug-like compound lipophilicity and plasma free fraction in monkey and human. *J Pharm Sci*. 2012;101:1028–1039.